Acta Materialia 237 (2022) 118153

Contents lists available at ScienceDirect

Acta Materialia

journal homepage: www.elsevier.com/locate/actamat

Full length article

Unexpected role of prefactors in defects diffusion: The case of vacancies in the 55Fe-28Ni-17Cr concentrated solid-solution alloys

Alecsandre Sauvé-Lacoursière[a], Simon Gelin[a,b,c], Gilles Adjanor[d], Christophe Domain[d], Normand Mousseau[a,*]

[a] Département de physique and Regroupement québécois sur les matériaux de pointe, Université de Montréal, Case Postale 6128, Succursale Centre-ville, Montréal, Québec H3C 3J7, Canada
[b] Département de mathématiques et de génie industriel, école Polytechnique de Montréal, Montréal, Québec H3C3A7, Canada
[c] Institut Lumière Matière, UMR 5306 Université Lyon 1-CNRS, Université de Lyon, Villeurbanne Cedex F-69622, France
[d] EDF Lab Les Renardières - Materials and Mechanics of Components departement, Moret-sur-Loing F-77818, France

ARTICLE INFO

Article history:
Received 15 March 2022
Revised 16 May 2022
Accepted 5 July 2022
Available online 7 July 2022

ABSTRACT

Variations in diffusion rates of simple point defects, such as vacancies and interstitials, are generally assumed to be dominated by energy barriers, as demonstrated for example by the large number of kinetic Monte Carlo studies that rest on constant rate prefactors. While this is mostly correct when energy barriers are well separated from each other, typically in crystals, entropic variations between the local minima and associated activated states become increasingly important as energy barriers of diffusion-mediating-mechanisms get closer, typically in disordered environments. The unexpected slower defect diffusion observed in high entropy alloys, which are characterized by the presence of a large number of different elements in roughly equal proportions, has brought us to revisit the role of prefactors. Combining the Activation-Relaxation Technique nouveau (ART nouveau) and the harmonic approximation for computing diffusion prefactors, we find that vacancy diffusion prefactors in a 55Fe-28Ni-17Cr concentrated solution alloy modeled with EAM empirical potentials can vary by up to six orders of magnitude, at almost constant energy barrier. This variation, mostly associated with changes in local pressure, suggests that prefactor could play a much more important role than previously thought in the defect kinetics of high entropy alloys and of disordered systems in general.

© 2022 Acta Materialia Inc. Published by Elsevier Ltd. All rights reserved.

1. Introduction

High-entropy alloys (HEAs) - containing five or more different atomic species at roughly equimolar concentrations - have attracted a large amount of scientific interest recently, sparked by their promising physical and mechanical properties. This discovery has revived the interest in concentrated solid solution alloys (CSAs) with more than two elements, as model alloys for fundamental investigations on HEA and also on more general complex concentrated alloys (CCA).

These random solid solutions, which can form single phase face-centered cubic (fcc) or body-centered cubic (bcc) crystals, have shown high resistance to ion irradiation [1] and possibly to corrosion [2,3]. Due to the richness of their composition, specific properties can be tuned by adjusting the concentration of the different components. For instance, enhancing the nickel proportion in iron-nickel-chromium alloys has been linked to the increase of their hardness while enhancing the percentage of chromium has been found to improve their oxidation resistance and, to some extent, also increase their hardness. These properties would make HEAs with a high ratio of nickel and chromium peculiarly well suited for uses in next-generation nuclear power plants.

Four mechanisms have been pointed out to explain the unique properties of these novel alloys, namely: the high entropy of the alloy (to a lesser extent in CSAs than in HEAs), the cocktail effect, a significant lattice distortion, and an observed sluggish internal diffusion [4]. These mechanisms remain debated in the literature, in part because a microscopic justification for these is still largely missing.

A particularly puzzling property of high-entropy alloys is the reduced defect diffusion rate with respect to pure systems [4], although this observation remains under debate [5–9]. Sluggish diffusion can be defined as "when the diffusion coefficients are smaller than those of pure metals and conventional alloys." (see Zhang et al. [10], for instance). As stated, this reduced diffusion

* Corresponding author.
E-mail address: normand.mousseau@Umontreal.ca (N. Mousseau).

https://doi.org/10.1016/j.actamat.2022.118153
1359-6454/© 2022 Acta Materialia Inc. Published by Elsevier Ltd. All rights reserved.

corresponds to a non-monotonic behavior (in fact, the presence of a minimum) of the tracer self-diffusion coefficients [11]. Using a variety of KMC detrapping techniques, with constant prefactor assumptions, Ferasat et al. concluded that this monotonic behavior could be explained, not only by geometric percolation, but also by composition and local environment dependence on migration energies. Other recent work suggests, rather, that this phenomenon cannot be explained by a change in the diffusion energy barrier due to the disorder. Recent experimental [12] results in particular have shown that both the vacancy enthalpy formation and diffusion activation energies are similar in the alloy and in the related pure metals. High-temperature molecular dynamics and low-temperature off-lattice kinetic Monte Carlo, using k-ART [13,14], with fixed prefactor, also found that vacancy diffusion coefficients in a binary NiFe alloy lied in between those of pure Ni and pure Fe. In addition, the results of these simulations suggest that, under irradiation, the microstructural evolution of concentrated alloys should be qualitatively different from that of dilute alloys [15]. Other recent simulations, also carried out with empirical potentials, showed a distribution of formation energies and diffusion barriers across the modelled samples, yet without clear link to diffusion [16].

In line with the general work on point defect diffusion in solids, while much attention has been given to understanding the effect of alloying in defect energy formation and activation barrier, most studies, including the KMC simulations mentioned above [11,15], assume that the diffusion prefactor varies little with respect to the exponential Boltzmann factor. Yet, recent experiments suggest that entropy affects diffusion in HEA [9]. Moreover, as demonstrated recently in amorphous and glassy materials, and as confirmed in this study, prefactors can exhibit a wide dispersion even for similar energy barriers [17].

In this work, we turn our attention to the reduced diffusion observed in these systems as compared with pure elements and explore how this observation could emerge from the variations in the energy landscape associated with chemical disorder. More specifically, we focus on the role of the diffusion prefactor, which is generally considered constant in point defect diffusion. Recent characterization of prefactors for large sets of barriers in glasses and amorphous systems, by some of us, has shown unexpected variations in this quantity for highly disordered materials [17]. While connecting these variations to atomic diffusion is extremely complex in amorphous solids, where diffusion proceeds from a wide diversity of local mechanisms, we expect such a connection to be more tractable in high entropy alloys. Indeed, being solid solutions, these solids have a much simpler energy landscape, and defect diffusion therein involves a finite set of mechanisms similar to those in pure crystalline systems.

To explore the role of diffusion prefactors, we model a 55Fe-28Ni-17Cr concentrated solution alloy using embedded-atom method empirical potentials (EAM). We use the Activation-Relaxation Technique (ART nouveau) [18,19] to sample the energy landscape and compute the transition rate Γ for each specific event using the harmonic Transition State Theory (hTST) [20].

In Section 2, we detail the simulation approach and the selected empirical potential used. The nature of the energy landscape, including energy barriers and prefactors, as well as correlation between those, are explored in Section 3. Finally, we discuss the significance of these results in Section 4.

2. Method

2.1. ART nouveau: identifying events and computing prefactors

Events are generated with the Activation Relaxation Technique nouveau (ARTn) [18,19,21], with force calculations obtained through LAMMPS running as a library [22,23]. Displacements centered on all first, second and third-neighbour atoms surrounding a vacancy are generated in random directions to build an extensive catalog of events containing the initial, saddle and final configurations. For each event, the prefactor is computed within the harmonic approximation as described in Eq. (2) or given a constant value of $10^{13}s^{-1}$.

The use of a fixed prefactor, or attempt frequency, set around $10^{13}s^{-1}$, is a simplification that has been shown to hold in several systems, including for the ab initio study of vacancy diffusion in Si [24], relaxation mechanisms in Stillinger-Weber amorphous silicon [25], and adatom diffusion on Cu and Ag surfaces [26]. More specific to the system of interest here, it is also compatible with pre-exponential factors for diffusion in iron obtained both from experiments [27] and simulations [28].

Combining the prefactor with the energy barriers, we obtain the total rate associated with moving out of the current configuration. To facilitate the management of the catalog and ensure that specific events are only counted once, we use, more specifically, the kinetic Activation-Relaxation Technique (k-ART) package [13,14] and launch 10 event searches per unique topology for atoms surrounding the vacancy. This value ensures a rich sampling of the energy landscape surrounding the vacancy.

The harmonic Transition State Theory (hTST) [20] defines the transition rate as a function of temperature T as

$$\Gamma(T) = \nu_{hTST} e^{-\frac{(E_S - E_m)}{k_B T}}, \tag{1}$$

where and E_s and E_m are the configurational energies at the saddle point and the minimum, and ν_{hTST}, the hTST attempt frequency, is given by

$$\nu_{hTST} = \frac{\prod_{i=1}^{N} \nu_i^m}{\prod_{i=1}^{N-1} \nu_i^s} \tag{2}$$

where ν_i^s and ν_i^m, are real vibrational frequencies at the saddle point and the minimum, respectively, and are obtained by computing the dynamical matrix

$$D_{i\alpha j\beta} = \frac{1}{\sqrt{m_i m_j}} \frac{\partial^2 V}{\partial x_{i,\alpha} \partial x_{j,\beta}} \tag{3}$$

where i, j run over all atoms, α, β are the cartesian coordinates (x, y, z), V is the interaction potential, and m_i the atomic mass.

In this paper, the matrix is obtained through a centered-finite difference formulate with small finite displacements of 0.01 Å, for this potential, selected to converge the prefactor. The exact step size for this discrete derivative depends on the roughness and cut-offs of the potential. In this cases displacements within a factor two around this value give the same result. Frequencies correspond to the square root of the dynamical matrix eigenvalues.

2.2. Simulated systems

A cubic box of a face-centered cubic high-entropy solid solution alloy of 2048 atoms (8 x 8 x 8 cells), with periodic boundary conditions, is generated by randomly placing iron, nickel and chromium atoms on the lattice in a proportion of 55% of iron (1126 atoms), 28% of nickel (573 atoms) and 17% of chromium (349 atoms). The resulting system is then relaxed statically at $T = 0$ and $P = 0$ with LAMMPS resulting in a lattice constant of 3.5501Å.

One atom is removed at random from the simulation box to create a vacancy. This process is repeated 22 times leading to 22 different cells of 2047 atoms with one vacancy each.

Each of the 22 systems is evolved for 1 KMC step. Such step encompasses the construction of the respective event catalog associated with each specific vacancy configuration for a total of 243

Table 1
Chemical potential of each species in the studied concentrated solid-solution alloys (CSA) and in the pure substance (PS) computed with the procedure developed in Ref. [32].

	Chemical Potential (eV)	
Element	CSA	PS
Fe	-4.34 ± 0.02	-4.399
Ni	-4.41 ± 0.02	-4.446
Cr	-3.49 ± 0.02	-4.199

events, the computation of prefactors for all these events, the evaluation of a time step the selection of an event with the appropriate probability and the execution of this event. Here, we focus only on the event catalog and associated prefactors. These catalogs include mostly first-neighbor jumps into the vacancy, as well as some more complex events. Only events with a barrier less than 5 eV are included. These catalogs form the basic data set for analysing the variations of pre-exponential factors and transition rates with the type of vacancy created and its local environment at the initial minimum and the saddle point.

2.3. Empirical potential

Among the most popular Embedded Atom Method (EAM) potentials for the iron-nickel-chromium alloy, the FeNiCr-2011 [29] and the FeNiCr-2013 potentials [30], both from Bonny *et al.*, are often considered. Both potentials reproduce very well the cohesive energies and elastic constants experimental and DFT values for a large selection of FeNiCr compositions. The first potential also reproduces very well the stacking fault energies and it was originally designed to study the mobility of dissociated dislocations in the 70Fe-10Ni-20Cr alloy. The second potential is less reliable to that concern, as it was rather optimized for the diffusion of point defects in the same alloy: for selected compositions, formation energies of points-defects and their clusters are well reproduced, as well as the expected hierarchy of self-diffusion coefficients $D_{Cr} > D_{Ni} > D_{Fe}$ and their evolution with composition [30,31]. For this reason, we select the Bonny *et al.* FeNiCr-2013 EAM potential.

2.4. Formation energy

To compute the formation energy, we first compute the chemical potential for species in the alloy. To do so, we follow the procedure developed by some of us in Piochaud et al. [32]. Unlike in [32], however, here we compute the energy of every possible atomic switch. Thus, the minimal energy of the distributions used are not estimates but the real minimum of the distributions. These values are then used to compute the formation energy of the vacancies and errors are estimated by recomputing the values using the second lowest energy in the distribution. The chemical potential for each species computed in the solid solution and in a pure substance are presented in Table 1. The iron and nickel chemical potentials are only slightly higher in the alloy than in a pure substance while the chemical potential for the chromium is significantly larger in the alloy than in the pure substance. This indicates a segregation force for chromium.

3. Results

The exploration of the energy landscape associated with the jump of a single vacancy generated from the 22 different initial states produces 243 different events. These are defined by the initial state, the configuration at the saddle point and that at the final minimum. For each event, we compute the prefactor within the scope of the harmonic Transition State Theory (hTST), as described previously.

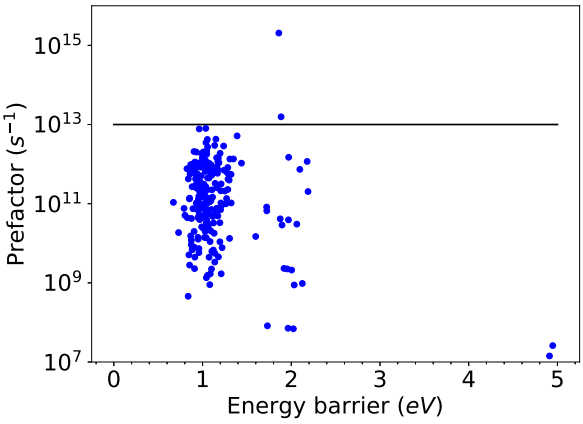

Fig. 1. Prefactor computed within the scope of the harmonic Transition State Theory plotted against the energy barrier of the event. The black line represents the prefactor value (10^{13} s^{-1}) typically used in KMC simulations.

Fig. 1 plots the hTST prefactor as a function of the energy barrier of the events. Three groups of barriers can be distinguished. A first one, around 1 eV is associated with the jump of the vacancy to a nearest-neighbour site. The barriers around 2 eV include either jumps to unstable positions or to a first-neighbour site, through a higher energy barrier; finally, the events at 5 eV, just below the barrier threshold that we use to focus on the lower energy barrier events, is associated with a jump to a second-neighbour site through a high-barrier saddle point.

We observe a wide distribution of prefactors within each category of jumps, with prefactors varying by up to four orders of magnitudes for events around 1 eV and more than 6 orders of magnitude for events of similar barriers around 2 eV. For example, the jump of a chromium atom over a 0.882 eV barrier is associated with a transition rate of $8.7 \times 10^8 s^{-1}$, while two other events with close (low) barriers and associated with Fe and Ni diffusion, respectively, are activated at rates of $342 \times 10^8 s^{-1}$ and $1225 \times 10^8 s^{-1}$, respectively. This difference in prefactors is also observed for vacancies of the same atom species: two similar events involving a Fe jumping, with a barrier of 0.913 eV, have a rate that differs by a factor of more than 300.

While the dispersion is broader for events around 2 eV, the prefactors just below 5 eV are particularly low. This suggests an anti Meyer-Nelder law, or negative enthalpy-entropy compensation, as observed for some metallic alloys in Ref. [17], where it was shown that this relation holds in average, while allowing large dispersion in small energy barrier intervals.

Within the harmonic approximation, the prefactor is determined by the ratios of vibrational frequencies at initial minimum over vibrational frequencies at the saddle point. The change of vibrational frequencies under a local deformation is an intricate function of the interatomic interactions, the solid's microstructure and the deformation features, so in view of identifying the main factors that contribute to the observed dispersion of prefactors, we start by looking for possible correlations with chemical and structural properties of local environments.

We replot the prefactor vs. energy barrier figure with events now colored according to the number of Fe (Fig. 2, top panel), Ni (middle panel) and Cr (bottom panel) atoms in the first shell surrounding the vacancy, and with the two points around 5 eV removed to focus on the lower barriers. These figures show the wide variation of initial local environments for the 22 simulated cells: the number of Fe atoms in the first shell varies between 2 and 9 among the 12 first neighbours, that of nickel between 0 and 8 and

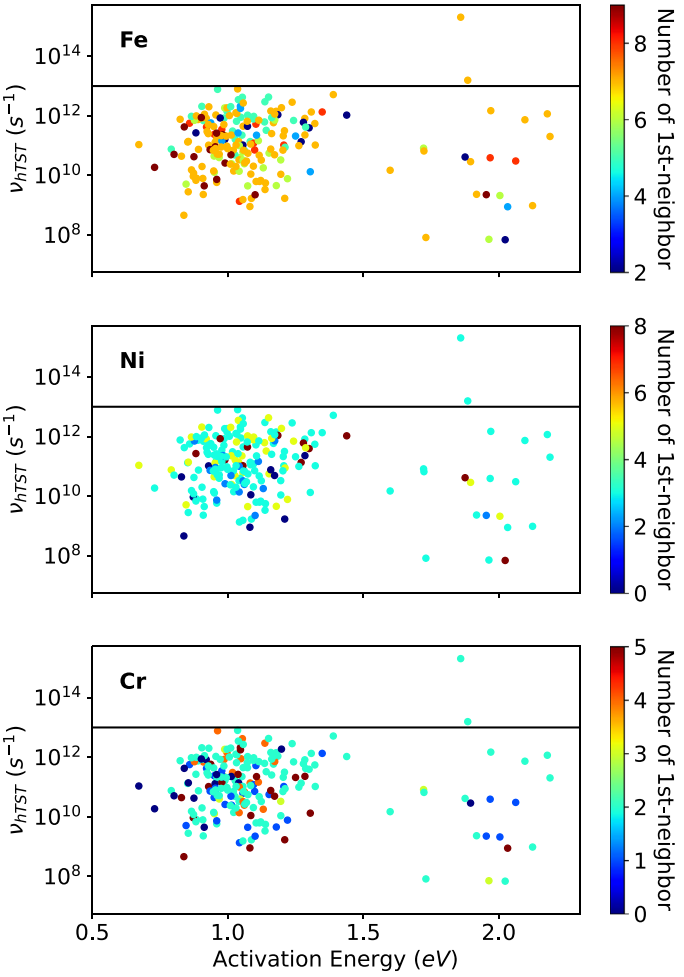

Fig. 2. hTST prefactor plotted against the energy barrier of the event. The points are colored as a function of the number of Fe atoms (top panel), Ni atoms (middle panel) and Cr atoms (bottom panel) in 1st neighbor position around the vacancy. The black line represents the prefactor value (10^{13} s^{-1}) typically used in KMC simulations.

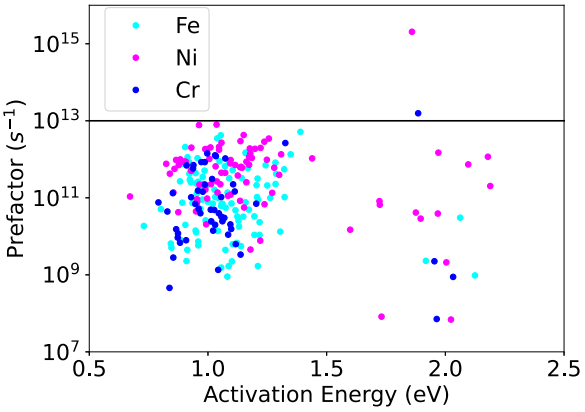

Fig. 3. hTST prefactors (s^{-1}) as a function event barrier (eV) for vacancy diffusion events in a 55Fe-28Ni-17Cr high entropy alloy, starting from 22 different initial configurations. The points in blue represent Cr atoms moving in the vacancy site, in red Fe atoms and those in green Ni atoms. (For interpretation of the references to color in this figure legend, the reader is referred to the web version of this article.)

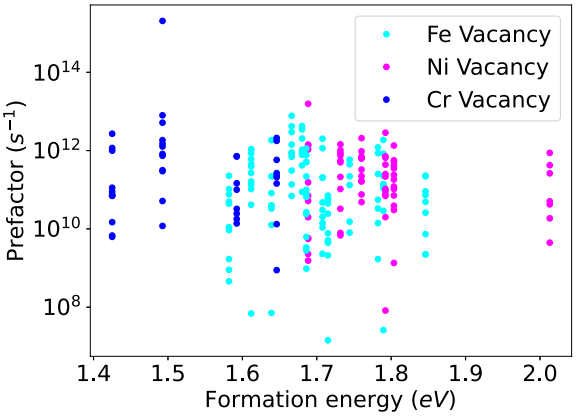

Fig. 4. hTST prefactor as a function of the vacancy formation energy for the 22 cells created. The points in blue represent Cr vacancies, in red Fe vacancies, and those in green Ni vacancies. (For interpretation of the references to color in this figure legend, the reader is referred to the web version of this article.)

that of chromium between 0 and 5. They do not show any correlation between prefactors and the chemical environment in the first shell surrounding the vacancy.

We did not find any more correlation when looking at the environment beyond the first vacancy shell up to the 2nd, 3rd and 4th neighbors of the vacancy (not shown, as they are similar to those presented for the first neighbour shell). We also observed the same absence of correlation between the prefactor and the chemical nature of the diffusing atom (Fig. 3).

We now evaluate whether the hTST prefactor is influenced by the formation energy of the vacancies, which offers a measure of the local strain. Fig. 4 represents prefactors as a function of vacancy formation energies. Each vertical row of points of a given color represents the prefactor values of every event found in one of the 22 initial systems. As previously, we find no correlation between the value of the computed prefactor and the formation energy of the vacancies: from the same energy minimum, the prefactor value can vary by multiple orders of magnitude independently of the formation energy.

Altogether, the absence of correlation between the prefactor and the local minimum structure, whether characterized through vacancy formation energy, nature of the vacancy or local chemical environment, suggests that the origin of the wide dispersion of rate prefactors cannot be simply explained by the local environment in this system.

The spread in the hTST prefactor for events starting from the same local environment can only be explained by variations in the vibrational spectrum at the saddle point, which appears at the denominator in Eq. (1). While the chemical nature of the atoms moving into the vacancy could affect the lattice at the saddle point and, therefore, the vibrational spectrum, a plot of the prefactor as a function of energy barrier and the chemical nature of the atom diffusing into the vacancy, shown Fig. 3, does not reveal obvious correlations between the diffusing atom and the prefactor. This suggests that correlations are associated with a more global quantity.

To capture this effect, we evaluate the local pressure around the vacancy at the saddle point using LAMMPS to extract the stress tensor of the atoms within 4 Å of the defect. The stress tensor is then used to compute the local pressure at this point. The prefactor value is plotted against the local pressure at the saddle point on Fig. 5 and shows a clear correlation in spite of significant dispersion. Negative pressure associated with a "pull" on the local atoms leads to a higher prefactor, while a positive pressure, indicative of a local environment under compression, comes with lower prefactors on average.

This correlation between pressure and prefactor is compatible with a recent analysis of the physical origin of the enthalpy-entropy compensation law [17]. Building on a millions of events

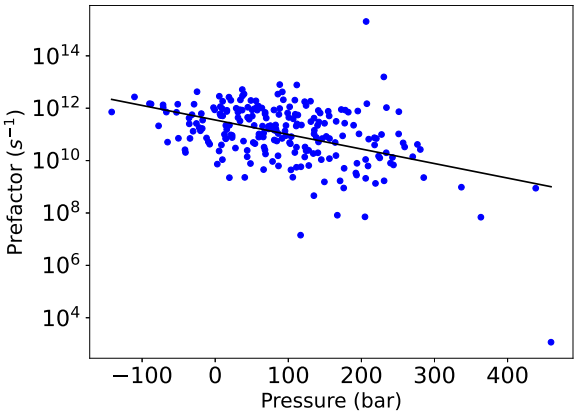

Fig. 5. hTST prefactor against the local pressure at the saddle point. The pressure is computed on every atom within 4Åof the defect.

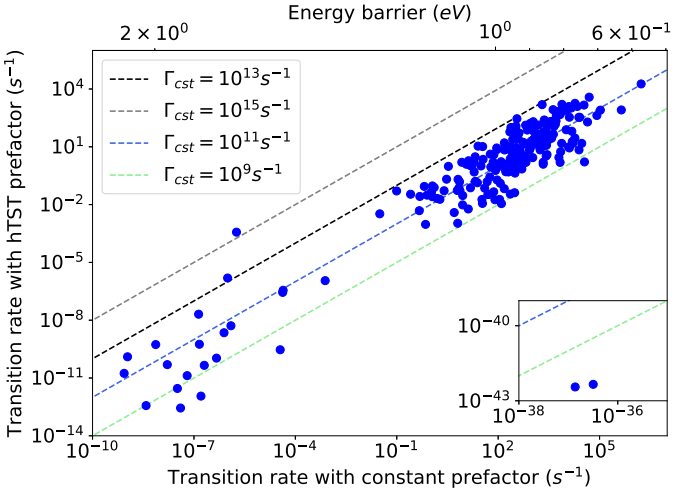

Fig. 6. Transitions rates including the hTST prefactor plotted as a function of transition rates computed with a constant prefactor (bottom axis) and events energy barriers (top axis). The dashed black line shows where the points would fall if rates computed with the hTST method were equal to the ones computed with a constant prefactor of 10^{13} s^{-1}. The dark cyan, dark green and light green represent the same situation but with a constant prefactor of respectively 10^{15} s^{-1}, 10^{11} s^{-1} and 10^{9} s^{-1}. The inset shows two data points with an energy barrier around 5 eV with the dark green and light green lines described previously. (For interpretation of the references to color in this figure legend, the reader is referred to the web version of this article.)

computed on four different systems, it was shown that compression at the saddle point leads to shifts in the vibrational frequencies to higher values and, therefore, a decrease in the prefactor. Because a number of parameters impact the vibrational spectrum, this trend is only true on average, with considerable dispersion associated with more subtle effects associated with the specificities of the local environment.

4. Discussion and conclusion

Here, we examined the diversity of prefactors in a concentrated alloy representing a solid solution of high entropy model alloy composed of similar size atoms using an empirical potential adjusted to reproduce the point defect formation energy and diffusion [30]. Because of this similarity, diffusion prefactors for a vacancy in this system could be assumed to show relatively small dispersion when compared to that observed in glasses. Yet, as shown in Fig. 2, which plots the prefactor as a function of energy barrier, and Fig. 6, which shows the total rates including the hTST prefactor, as defined by Eq. (1), against the ones computed with a constant prefactor (bottom axis) and the energy barrier (top axis), the distribution of prefactors for similar barriers is quite broad, reaching four to six orders of magnitude, and is centered around an average prefactor of $10^{11} s^{-1}$, significantly lower than the $10^{12} - 10^{13} s^{-1}$ normally used in KMC simulations.

Detailed analysis demonstrates that it is difficult to link the variation in prefactors to precise geometric and chemical properties as there are no manifest correlations with the chemical identify of diffusing atoms nor with the local environment surrounding the vacancy, which suggests that a combination of factors are at play here. Indeed, only the local pressure at the saddle point, does indicate some degree of correlation, with increasing local pressure decreasing prefactor. This result indicates that the variation in prefactors is controlled, at least in part, by the deformations at the saddle point, irrespective deformations at the initial minimum. It is compatible with the conclusions from recent study of the law of compensation in glasses and amorphous systems [17,33] where dense and rigid systems, such as Lennard-Jones glasses, were shown to display an anti-compensation behavior controlled by the nature of the saddle point.

The large distribution of transition rates around a given defect for similar mechanisms and barriers inevitably impacts the diffusion kinetics in high entropy systems. Indeed, it introduces significant biases in the sampling of events with similar energy barriers: as can be seen in Fig. 6, a particular event might be activated once every 10,000 times compared to an event with almost the exact same barrier when taking into account the hTST prefactor. Therefore, while an error on the transition rate only affects the value of the diffusion coefficient in a pure element system, where diffusion proceeds through a single mechanism, discarding variations of prefactors in high entropy alloys will most likely lead to unrealistic diffusion pathways. More work is needed to fully assess how the distribution of prefactors impact kinetic measurements.

In itself, this observation calls for more detailed analyses of the variations of prefactors around point and extended defects in complex solids and demonstrates the importance of taking them into account when describing the temporal evolution of these materials. For the alloy studied here, it raises the possibility that the observed slowing down of self-defect diffusion in high-entropy alloys could be associated with entropic variations along the diffusion pathways, rather than energetic fluctuations. To fully address this question, extended kinetic simulations will be necessary and will be undertaken in a future work.

Code and data availability

The ARTn and kinetic ART packages as well as the data reported here are distributed freely. Please contact Normand Mousseau (normand.mousseau@umontreal.ca).

Declaration of Competing Interest

The authors declare no conflict of interest.

Acknowledgments

This work was supported in part by the Materials Ageing Institute Scientific Network (MAI-SN). NM acknowledges partial support through a Discovery grant from the Natural Science and Engineering Research Council of Canada. We are grateful to Calcul Québec and Compute Canada for generous allocation of computational resources.

References

[1] N.K. Kumar, C. Li, K. Leonard, H. Bei, S. Zinkle, Microstructural stability and mechanical behavior of Fenimncr high entropy alloy under ion irradiation,

Acta Mater. 113 (2016) 230–244, doi:10.1016/j.actamat.2016.05.007. URL: https://www.sciencedirect.com/science/article/pii/S1359645416303342.
[2] Y. Shi, B. Yang, P. Liaw, Corrosion-resistant high-entropy alloys: areview, Metals 7 (2) (2017) 43, doi:10.3390/met7020043. URL: http://www.mdpi.com/2075-4701/7/2/43.
[3] Y. Qiu, S. Thomas, M.A. Gibson, H.L. Fraser, N. Birbilis, Corrosion of high entropy alloys, npj Mater. Degrad. 1 (1) (2017) 15, doi:10.1038/s41529-017-0009-y. URL: http://www.nature.com/articles/s41529-017-0009-y.
[4] K.-Y. Tsai, M.-H. Tsai, J.W. Yeh, Sluggish diffusion in Co–Cr–Fe–Mn–Ni high-entropy alloys, Acta Mater. 61 (13) (2013) 4887–4897, doi:10.1016/j.actamat.2013.04.058. URL: https://linkinghub.elsevier.com/retrieve/pii/S1359645413003431.
[5] D. Miracle, O. Senkov, A critical review of high entropy alloys and related concepts, Acta Mater. 122 (2017) 448–511, doi:10.1016/j.actamat.2016.08.081. URL: https://linkinghub.elsevier.com/retrieve/pii/S1359645416306759.
[6] M. Vaidya, G.M. Muralikrishna, S. Divinski, B. Murty, Experimental assessment of the thermodynamic factor for diffusion in CoCrFeNi and CoCrFeMnNi high entropy alloys, Scr. Mater. 157 (2018) 81–85, doi:10.1016/j.scriptamat.2018.07.040. URL: https://linkinghub.elsevier.com/retrieve/pii/S1359646218304676.
[7] S.V. Divinski, A.V. Pokoev, N. Esakkiraja, A. Paul, A mystery of "sluggish diffusion" in high-entropy alloys: the truth or a myth? DF 17 (2018) 69–104, doi:10.4028/www.scientific.net/DF.17.69. URL: https://www.scientific.net/DF.17.69.
[8] J. Dąbrowa, M. Danielewski, State-of-the-art diffusion studies in the high entropy alloys, Metals 10 (3) (2020) 347, doi:10.3390/met10030347. URL: https://www.mdpi.com/2075-4701/10/3/347.
[9] D. Gaertner, J. Kottke, Y. Chumlyakov, F. Hergemöller, G. Wilde, S.V. Divinski, Tracer diffusion in single crystalline CoCrFeNi and CoCrFeMnNi high-entropy alloys: kinetic hints towards a low-temperature phase instability of the solid-solution? Scr. Mater. 187 (2020) 57–62, doi:10.1016/j.scriptamat.2020.05.060. URL: https://linkinghub.elsevier.com/retrieve/pii/S1359646220303493.
[10] Y. Zhang, T. Egami, W.J. Weber, Dissipation of radiation energy in concentrated solid-solution alloys: unique defect properties and microstructural evolution, MRS Bull. 44 (10) (2019) 798–811, doi:10.1557/mrs.2019.233. URL: http://link.springer.com/10.1557/mrs.2019.233.
[11] K. Ferasat, Y.N. Osetsky, A.V. Barashev, Y. Zhang, Z. Yao, L.K. Béland, Accelerated kinetic monte carlo: a case study; vacancy and dumbbell interstitial diffusion traps in concentrated solid solution alloys, J. Chem. Phys. 153 (7) (2020) 074109, doi:10.1063/5.0015039. URL: https://doi.org/10.1063/5.0015039.
[12] K. Sugita, N. Matsuoka, M. Mizuno, H. Araki, Vacancy formation enthalpy in CoCrFeMnNi high-entropy alloy, Scr. Mater. 176 (2020) 32–35, doi:10.1016/j.scriptamat.2019.09.033. URL: https://linkinghub.elsevier.com/retrieve/pii/S1359646219305676.
[13] F. El-Mellouhi, N. Mousseau, L.J. Lewis, Kinetic activation-relaxation technique: an off-lattice self-learning kinetic Monte Carlo algorithm, Phys. Rev. B 78 (15) (2008) 153202, doi:10.1103/PhysRevB.78.153202. URL: http://link.aps.org/doi/10.1103/PhysRevB.78.153202.
[14] L.K. Béland, P. Brommer, F. El-Mellouhi, J.-F. Joly, N. Mousseau, Kinetic activation-relaxation technique, Phys. Rev. E 84 (4) (2011) 046704, doi:10.1103/PhysRevE.84.046704. URL: http://normandmousseau.com/publications//130.pdf.
[15] Y.N. Osetsky, L.K. Béland, R.E. Stoller, Specific features of defect and mass transport in concentrated FCC alloys, Acta Mater. 115 (2016) 364–371, doi:10.1016/j.actamat.2016.06.018. URL: https://linkinghub.elsevier.com/retrieve/pii/S1359645416304372.
[16] W.-M. Choi, Y.H. Jo, S.S. Sohn, S. Lee, B.J. Lee, Understanding the physical metallurgy of the CoCrFeMnNi high-entropy alloy: an atomistic simulation study, npj Comput. Mater. 4 (1) (2018) 1, doi:10.1038/s41524-017-0060-9. URL: http://www.nature.com/articles/s41524-017-0060-9.
[17] S. Gelin, A. Champagne-Ruel, N. Mousseau, Enthalpy-entropy compensation of atomic diffusion originates from softening of low frequency phonons, Nat. Commun. 11 (1) (2020) 3977, doi:10.1038/s41467-020-17812-2. URL: https://doi.org/10.1038/s41467-020-17812-2.
[18] G.T. Barkema, N. Mousseau, Event-based relaxation of continuous disordered systems, Phys. Rev. Lett. 77 (21) (1996) 4358–4361, doi:10.1103/PhysRevLett.77.4358. URL: http://normandmousseau.com/publications/19.pdf.
[19] R. Malek, N. Mousseau, Dynamics of lennard-jones clusters: acharacterization of the activation-relaxation technique, Physical Review E 62 (6) (2000) 7723–7728, doi:10.1103/PhysRevE.62.7723. URL: http://link.aps.org/doi/10.1103/PhysRevE.62.7723.
[20] G.H. Vineyard, Frequency factors and isotope effects in solid state rate processes, J. Phys. Chem. Solids 3 (1) (1957) 121–127, doi:10.1016/0022-3697(57)90059-8.
[21] N. Mousseau, L.K. Béland, P. Brommer, J.-F. Joly, F. El-Mellouhi, E. Machado-Charry, M.-C. Marinica, P. Pochet, The activation-relaxation technique: ART nouveau and kinetic ART, J. At. Mol. Opt. Phys. (2012) 925278, doi:10.1155/2012/925278. URL: http://normandmousseau.com/publications/137.pdf.
[22] S. Plimpton, Fast parallel algorithms for short-range molecular dynamics, J. Comput. Phys. 117 (1) (1995) 1–19.
[23] ????, (????). LAMMPS web site, http://lammps.sandia.gov.
[24] F. El-Mellouhi, N. Mousseau, P. Ordejón, Sampling the diffusion paths of a neutral vacancy in silicon with quantum mechanical calculations, Phys. Rev. B 70 (2004) 205202, doi:10.1103/PhysRevB.70.205202. URL: https://link.aps.org/doi/10.1103/PhysRevB.70.205202.
[25] Y. Song, R. Malek, N. Mousseau, Optimal activation and diffusion paths of perfect events in amorphous silicon, Phys. Rev. B 62 (23) (2000) 15680–15685, doi:10.1103/PhysRevB.62.15680.
[26] H. Yildirim, A. Kara, T.S. Rahman, Origin of quasi-constant pre-exponential factors for adatom diffusion on cu and ag surfaces, Phys. Rev. B 76 (2007) 165421, doi:10.1103/PhysRevB.76.165421. URL: https://link.aps.org/doi/10.1103/PhysRevB.76.165421.
[27] J.A. Stroscio, D.T. Pierce, Scaling of diffusion-mediated island growth in iron-on-iron homoepitaxy, Phys. Rev. B 49 (1994) 8522–8525, doi:10.1103/PhysRevB.49.8522. URL: https://link.aps.org/doi/10.1103/PhysRevB.49.8522.
[28] N. Papanicolaou, H. Chamati, Diffusion of a vacancy on fe(100): amolecular-dynamics study, Comput. Mater. Sci 44 (4) (2009) 1366–1370, doi:10.1016/j.commatsci.2008.09.006. URL: https://www.sciencedirect.com/science/article/pii/S092702560800414X.
[29] G. Bonny, D. Terentyev, R.C. Pasianot, S. Poncé, A. Bakaev, Interatomic potential to study plasticity in stainless steels: the FeNiCr model alloy, Model. Simul. Mater. Sci. Eng. 19 (8) (2011) 085008, doi:10.1088/0965-0393/19/8/085008. URL: https://doi.org/10.1088/0965-0393/19/8/085008.
[30] G. Bonny, N. Castin, D. Terentyev, Interatomic potential for studying ageing under irradiation in stainless steels: the FeNiCr model alloy, Model. Simul. Mater. Sci. Eng. 21 (8) (2013) 085004, doi:10.1088/0965-0393/21/8/085004. URL: https://iopscience.iop.org/article/10.1088/0965-0393/21/8/085004.
[31] S. Zhao, G.M. Stocks, Y. Zhang, Defect energetics of concentrated solid-solution alloys from ab initio calculations: $Ni_{0.5}Co_{0.5}$, $Ni_{0.5}Fe_{0.5}$, $Ni_{0.8}Fe_{0.2}$ and $Ni_{0.8}cr_{0.2}$, Phys. Chem. Chem. Phys. 18 (34) (2016) 24043–24056, doi:10.1039/C6CP05161H. URL: http://xlink.rsc.org/?DOI=C6CP05161H.
[32] J.B. Piochaud, T.P.C. Klaver, G. Adjanor, P. Olsson, C. Domain, C.S. Becquart, First-principles study of point defects in an FCCFe-10Ni-20Cr model alloy, Phys. Rev. B 89 (2) (2014) 024101, doi:10.1103/PhysRevB.89.024101. URL: https://link.aps.org/doi/10.1103/PhysRevB.89.024101.
[33] P. Koziatek, J.-L. Barrat, P. Derlet, D. Rodney, Inverse meyer-neldel behavior for activated processes in model glasses, Phys. Rev. B 87 (22) (2013) 224105, doi:10.1103/physrevb.87.224105.